EXTREME LIMB OBSERVATIONS OF Ba II λ 4554 AND Mg I λ 4571

ROBERT J. RUTTEN

Sterrewacht 'Sonnenborgh', the Astronomical Institute, Utrecht, The Netherlands

(Received 25 June, 1976)

Abstract. Profiles of the Ba II λ 4554 resonance line and the Mg I λ 4571 intercombination line are presented, observed near the limb of the Sun. They are obtained from eclipse spectrograms with good spectroscopic resolution and an accurate height calibration. The reduction of the observations is described and detailed profiles are given for a range of viewing angles ($1/\cos\theta = 4-22$).

1. Introduction

In this paper eclipse observations of the Ba II λ 4554.0 resonance line and the Mg I λ 4571.1 intercombination line are presented. These lines are valuable probes of the solar atmosphere. The Ba II λ 4554 line ($6\,^2S_{1/2} - 6\,^2P^0_{3/2}$) is the only readily observable Ca II K-like resonance line other than H and K. This line is formed around the temperature minimum and is particularly sensitive to non-thermal broadening, i.e. collisional damping and large-scale motions. The Mg I λ 4571 line ($3\,^1S_0 - 3\,^3P^0_1$) has well-known diagnostic value based on its LTE source function. The relative populations of its upper and lower levels are completely controlled by collisions, so that their ratio is in LTE throughout the photosphere; at most small deviations occur in the chromosphere (Athay and Canfield, 1969; Altrock and Canfield, 1974). This property has been exploited in various analyses (e.g. Altrock and Cannon, 1972, 1973a, b, 1975; Rutten, 1973). Disk observations of this line with high spectral resolution have been given by White *et al.* (1972).

Observations of these lines at the extreme limb have the advantage – as for other lines – that the center-to-limb variation is extended with its extreme range, where the change in the height of line formation is much larger while the change in viewing angle is much smaller than on the disk. Line profiles observed at the limb are therefore valuable in the analysis of line formation (cf. Wijbenga and Zwaan, 1972). However, detailed line profiles from the limb have never been published.

For the chromospheric spectrum the most extensive material presently available is the tabulation of integrated line strengths by Dunn *et al.* (1968). For high layers knowledge of line strengths rather than profiles does not represent a severe limitation since the lines become optically thin and display simply the decline of their upper-level population density. But for most lines the disk profiles are not very sensitive to these chromospheric layers so that such data do not give constraints on the formation of lines observed on the disk.

Solar Physics **51** (1977) 3–24.

Closer to and within the limb resolved profiles are needed. Such profiles must be obtained during an eclipse. Extreme limb observations outside eclipses yield even in optimal seeing conditions qualitative information only, due to disk straylight and the unreliability of the height calibration (cf. Livingston and White, 1974). These problems can be overcome in eclipse observations, where the Moon supplies a complete cutoff of disk straylight as well as a reliable position indicator. However, it is difficult to record line profiles of good quality in the few seconds available.

This paper presents detailed line profiles from the extreme limb for the first time. The observations were obtained at Miahuatlan, Mexico, by the Dutch expedition to the March 7, 1970 eclipse.

The observing program, the instrumentation and the eclipse spectrograms are described elsewhere (Houtgast, Namba and Rutten, 1976; henceforward called Paper I). In the present paper the reduction procedures are discussed and the results for the λ 4554 and λ 4571 lines are given.

2. Observations

A slit-spectrograph was used to photograph the spectrum of the extreme limb of the Sun.

Earlier, slit-spectrographs were applied at eclipses only by Redman (1943, 1955). The use of the slit ensured maximal spectral resolution independent of image degradation by seeing or by errors in guiding or focus of the telescope. A coelostat followed the Moon accurately; the wavelength range 4545–4579 Å was photographed at a dispersion of 1.7 Å mm^{-1} on 70-mm Eastman Kodak Tri X film. Further details are given in Paper I.

Twenty-eight spectrograms were obtained just prior to second contact. They are listed in Table I. Reproductions of selected spectrograms are shown in Paper I. The determination of the height scale will be discussed in section 3. At the start of the series the spectrograms are slightly overexposed due to seeing excursions of the image on the spectrograph slit. These resulted in temporary occultations by the Moon of the aperture of a photomultiplier that was placed in the spectrum and controlled the exposures. It did not measure the whole width of the spectrum, but only a small part transmitted by a slit placed parallel to the dispersion direction (cf. Paper I).

Unfortunately this aperture was more frequently occulted than the remainder of the spectral width (Figure 1). Towards the limb, the overexposure decreases because the solar crescent became so narrow that the seeing excursions caused occultations of the whole width of the spectrum. The occultations spoiled the absolute intensity calibration because the recorded exposure times are no longer a good measure of the incident intensity. (Spectrogram 19 is underexposed due to an error in the automatic exposure circuit.)

A qualitative description of the behaviour of various lines has been reported

earlier (Houtgast *et al.*, 1971). A not yet understood phenomenon is the tilt shown by all lines. Interpreted at first as an accidental rotation of the spectrograph slit, it may have a solar cause since similar tilts were noted later by Houtgast and Namba (1975) in 1973 spectrograms and in previous slitless eclipse observations.

The spectrograms do not show fine structure, except for two Bailey beads close to the limb.

3. Geometry of the Observations

Eclipse spectrograms from a slit-spectrograph do not contain distinct position information in the spectrograms themselves; separate event registration is necessary to obtain an accurate calibration of the height scale of the observations. (Height is defined here as the projected radial distance above the solar limb.) A slit-jaw movie camera, a strip chart chronograph and two tape recorders were used (cf. Paper I).

The tapes were read out on paperchart with a multichannel UV recorder at high speed (29 cm s^{-1}). The moments of opening and closing of the shutter blades, the exposures of the slit-jaw movie (and various shouts of the observers) were determined in local (crystal-clock) time with a resolution of 1 ms; the calibration to UT using recorded radio time signals is accurate to within 3 ms. The exposure times are given in Table I.

The slit-jaw movie was used to determine the location of the slit on the solar image and the zero point of the height scale (i.e. the moment at which the projected solar limb crossed the slit).

The movie frames show the slit and the crescent very well. The individual mountains and valleys of the lunar limb are discernable in projection when the crescent breaks into beads. They can be identified with the details of the predicted lunar limb (Figure 1 of Paper I) by comparing the successive frames of the film, on which the lunar limb is scanned by the contracting horns of the solar crescent. Figure 1 shows two examples. The identification of the beads yielded the position angle of the slit during the observations. The slit was found to have been at 40.3° NESW, 13° away from the intended valley at contact point. Its orientation was nearly tangential to the limb, slanted at an angle of 18° (Figure 1).

Second contact took place at the expected position angle (27.5°). The predicted moment of contact was $17^h29^m03.5^s$ UT (Paper I), while the observed contact (last bead vanishes on the movie) was at $17^h29^m03.0^s \pm 0.3^s$ UT. However, an estimated value for ΔT (39.0^s) was used, and a correction must be applied for the 1.1″ deep valley. A prediction obtained afterwards with the definite value of ΔT (40.34^s) gave $17^h29^m01.7^s$ UT for the mean lunar diameter. Since the projected speed at which the valley was covered was 0.369″/s, the predicted disappearance of the last bead is at $17^h29^m04.7^s$, or 2.3^s later than observed. This difference points to a quite plausible error of 1–2 km in the coordinates of the site.

TABLE I
Eclipse spectrograms

Number of spectrogram	Begin of exposure		End of exposure	
	UT	Height (km)	UT	Height (km)
3	$17^h28^m9^s.16$	−13570	$17^h28^m9^s.19$	−13562
4	14.18	12178	14.28	12152
5	18.55	10966	18.70	10926
6	23.63	9559	23.69	9542
7	27.85	8388	27.92	8370
8	33.20	6905	33.31	6875
9	37.99	5575	38.09	5549
10	41.45	4916	41.62	4569
11	44.16	3867	44.39	3801
12	48.26	2729	48.41	2688
13	48.66	2618	48.83	2570
14	49.09	2500	49.29	2444
15	49.50	2385	49.74	2319
16	49.99	2249	50.20	2190
17	50.45	2120	50.74	2041
18	50.99	1971	51.20	1913
19	51.46	1842	51.58	1809
20	51.83	1739	52.31	1604
21	52.51	1551	52.93	1434
22	53.18	1365	53.52	1269
23	53.72	1198	54.36	1036
24	54.62	965	55.06	843
25	55.31	773	55.75	652
26	56.00	582	57.04	−294
27	57.28	−225	58.31	+58
28	58.56	+129	$17^h29^m07^s.22$	2529

The movie frames also show that the image of the Moon did not move relative to the slit during the half-minute prior to second contact in which all important spectrograms were taken.

The height scale of the spectrograms was derived from the observed moment of contact for the slit and the calculated speed at which the solar limb was covered there in the radial direction. At that moment and position angle the latter amounted to 0.385 ″/s or 277.3 km/s. The observed contact for the slit was at $17^h28^m58.1^s \pm 0.3^s$, which agrees with the prediction for this position angle ($17^h29^m00.3^s$) when the -2.3^s correction is applied.

The resulting heights for the spectrograms are entered in Table I. They are reliable to within 100 km (systematic error; their relative accuracy is much better).

The slit-jaw movie yields furthermore an estimate of the seeing. The diameter of the seeing disk was estimated to have been about 5″ or 3600 km on the Sun, from measurements of the extent of the smallest details along the projected lunar limb and of the radial widths of the beads at the moment that they disappear. The bad seeing is in agreement with the absence of fine structure in the spectrograms.

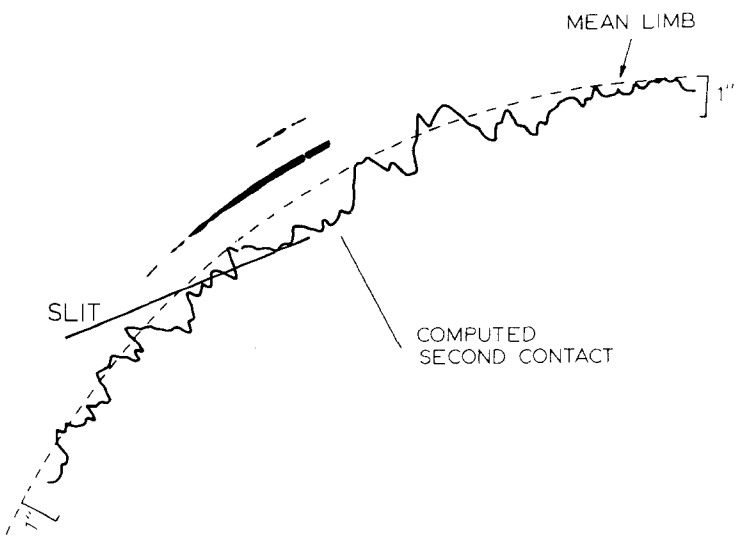

Fig. 1. Observed and predicted lunar limb at second contact. The radial scale of the predicted limb features is exaggerated fifty times. Two frames from the slit-jaw movie are superimposed. They were taken shortly before slit-contact and shortly before second contact, respectively. The predicted and observed features correspond very well. The slit is visible on the original frame. Its orientation is indicated at the predicted limb. The projected width of the slit was 0.73″ or 524 km on the Sun. The location on the slit corresponding to the aperture of the monitor photomultiplier in the spectrum is close to the mountain at which the slit intersects the lunar limb (this location was indicated by a needle, glued on the slit-jaw mirror, which is visible on earlier frames). The light line that intersects the crescent at right is a fiducial thread.

The observations do not represent the spectrum of the part of the disk covered by the slit only but a weighted mean of the contributions from all layers outside the lunar limb. This was confirmed by scans of the last spectrograms made in the Bailey beads and between the beads that show no differences in line profiles (after conversion into intensity) larger than their noise. The height values given in Table I therefore represent lower cutoffs of the contribution function only.

Hansen *et al.* (1970) have published Sacramento Peak H_α filtergrams and Mauna Loa coronagraph observations for 7 March 1970 and the surrounding days. They show no particular activity at the limb at the observed position angle. The large coronal streamer observed at about this position was based on an extended active region that passed the east limb already on 3 March.

4. Microphotometry

The spectrograms were scanned with the old Utrecht microphotometer (Houtgast, 1948). This double-slit instrument was updated by adding a Heidenhain position encoder and digital registration on punched paper tape, resulting in a measuring speed of 100 samples/s and a positional accuracy of 1 μm (Rutten and Van Amerongen, 1975). The spectrograms were cut from the film, clamped between

glass plates and measured at 4 μm intervals with projected slit widths of 6 μm. Because the microphotometer adjustments are not perfectly reproducible and also because small deviations of the focus over the travel length of the plateholder carriage produced variations in the measured transmission, the clear film along the spectrum was also scanned, averaged over short segments and used to normalize the spectrum transmission. Characteristic curves were determined from the numerous calibration spectrograms taken on the eclipse films before and after the eclipse and on the following day. Separate curves were constructed from spectrograms made with a 7-step weakener, with different combinations of neutral filters and with various telescope apertures, all for separate exposure times (0.4 s, 0.8 s and 2 s). The scatter in the individual curves was found to be rather large, especially for the step-weakener data since these contain the overlying center-to-limb variation of the solar image for which only coarse corrections could be applied. The differences between the curves for different exposure times are smaller than the scatter; therefore a single composite characteristic curve was derived, with extra weight given to the neutral filter data.

The uncertainty in the intensity calibration is largest for the continuum of the

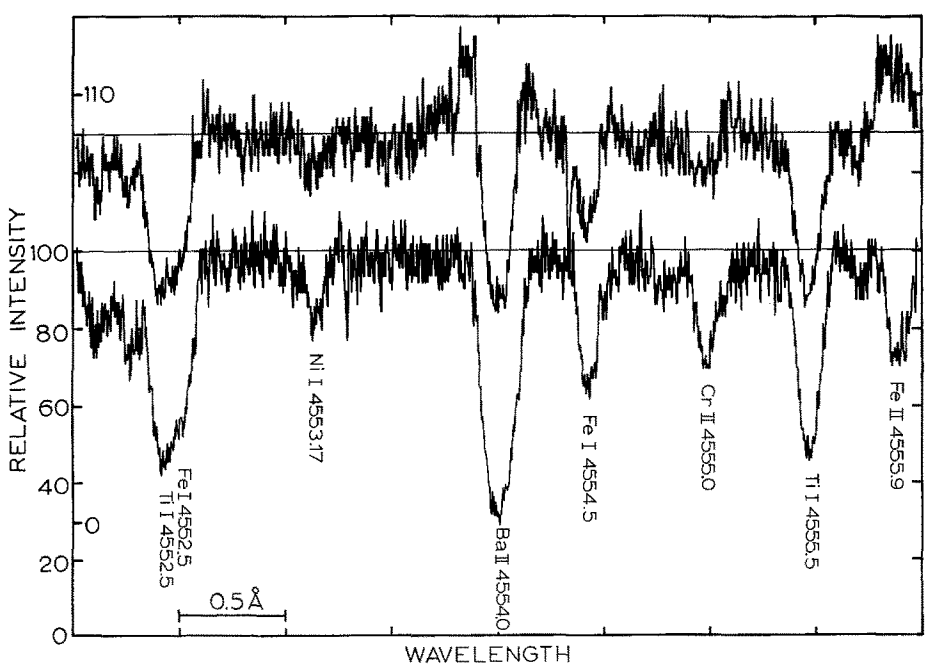

Fig. 2. Part of the tracings around 4554 Å from spectrogram 12 (bottom) and spectrogram 25 (top). Ordinate: relative intensity (continuum = 100) with a vertical offset of 30% for the top tracing. Abscissa: relative wavelength (zero-point unknown). Some identifications are indicated. Note the emission wings of Ba II λ 4554 and the emission profile of Fe II λ 4556 in the top tracing. The granularity of spectrogram 25 is less than for spectrogram 12, but shorter microphotometer slits had to be used for this spectrogram because of Bailey beads; the noise level is therefore similar.

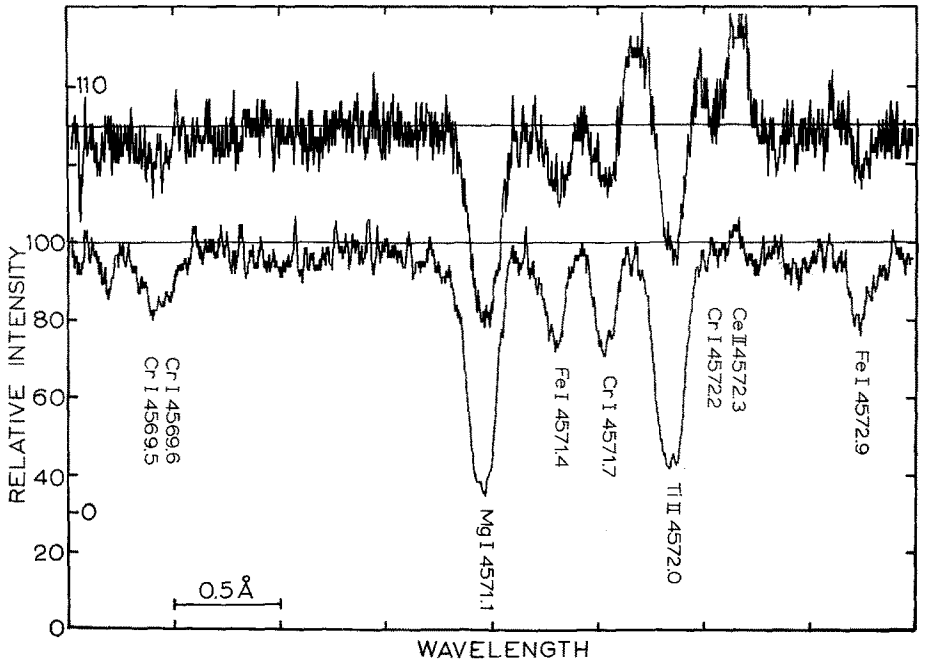

Fig. 3. Part of the tracings around 4571 Å from spectrogram 12 (bottom) and spectrogram 25 (top). Labeling as in Figure 2. The larger noise in the top tracing is due to shorter microphotometer slits. Note the emission wings of Ti II λ 4572.0 and the emission profile of Ce II λ 4572.3 in the top tracing.

early spectrograms due to their overexposure. These spectrograms show also an increasing density and graininess towards the short wavelength end. The calibration of the far wings of the λ 4554 line is therefore less reliable than for the λ 4571 line. However, the reliability increases towards the limb.

The profiles of both lines were scaled to hand-drawn continua, determined in the windows at 4553 Å and 4556.7 Å for the λ 4554 line and the windows at 4568 Å and 4573.5 Å for the λ 4571 line. The continuum fits for the λ 4554 profiles are hampered by less good windows and the increases of density and granularity towards the film edge of the early spectrograms. Corrections for spectrographic straylight are incorporated in the restoration procedure discussed below. Examples of rectified scans are given in Figures 2 and 3.

5. Restoration

The tracings are very noisy due to the graininess of the sensitive emulsion and distorted by the finite resolution of the spectrograph. The use of a slit during the eclipse had the advantage that the instrumental profile was not influenced by irreproducibles as telescope focus, guiding and atmospheric seeing, so that it could be determined separately. The λ 6328 line of a He–Ne laser was photographed at night with a wide range of neutral filters, in three different polarization directions (cf. Paper I).

The resulting spectrograms show many ghosts. These are doubled by internal reflection in the beam-splitter used to feed two film magazines with spectra of different intensity (90% reflected and 8% transmitted). The secondary image is negligible compared to the ghosts for the (reflected) eclipse spectrograms (relative intensity 7×10^{-6}), but in the red the beam-splitter coating was transparent so that the secondary image is appreciable in the transmitted laser spectra.

The laser spectrograms were scanned with the same microphotometer adjustments as the eclipse spectrograms, so that effects of sampling resolution are included in the restoration. The scans were converted into intensity with a separate characteristic curve for the red wavelength region and the short exposure times used. It was constructed from the neutral filter data and the secondary images. The instrumental profile was assembled by fitting logarithmic intensity plots from the various exposures together. No dependence on polarization was found. The test was made because the transmission of the spectrograph was very sensitive to the polarization of the incoming beam of light, and effects on the instrumental profile were feared from changes in grating illumination. A later analysis of the spectrograph of the McMath telescope at Kitt Peak by Breckinridge (1971) also showed a large influence of polarization on transmission due to Wood's anomalies, but only slight changes at most in the instrumental profile.

The instrumental profile thus found refers to 6328 Å while the eclipse spectra are centered on 4560 Å; transformation of the instrumental profile to this wavelength is necessary. The various contributions have different wavelength-dependence and must be scaled separately. The core of the measured profile at 6328 Å has a Gaussian shape while its wings show the familiar $(\Delta\lambda)^{-2}$ decay with superimposed ghosts (cf. Griffin, 1969). The core has a halfwidth of 34 μm (or 15.2 mÅ), in agreement with the expected value (spherical aberration of the collimator: 30 μm; grating resolution: 13 μm). The total wavelength-independent contribution (spherical aberration, diffusion in the emulsion, microphotometer resolution) was therefore assumed Gaussian in shape with a halfwidth of 31.5 μm or 18.6 mÅ at 4560 Å, while the grating contribution to the core, also Gaussian, was scaled in Å with the wavelength ratio. The resulting core at 4560 Å is Gaussian with a halfwidth of 32.4 μm or 19.1 mÅ. The $(\Delta\lambda)^{-2}$ wings with the ghosts were also scaled with the wavelength ratio and extrapolated to lower intensity levels using log-log plots. The resulting instrumental profile is given in Figure 4. It shows the common property of single-pass spectrographs that the halfwidth gives an overestimate of the resolving power (here $\approx 240\,000$) because the wide wings and the ghosts degrade the spectral purity appreciably. These are the chief sources of spectrograph straylight. Therefore the correction for straylight is best done by including the wings in the restoration procedure, especially when emission lines are present in an absorption spectrum.

The deconvolution of the observed spectra with the instrumental profile was achieved by dividing their Fourier transforms, using the ALGOL '60 Fast Fourier Transform procedure given by Singleton (1968). Deconvolution by direct Fourier

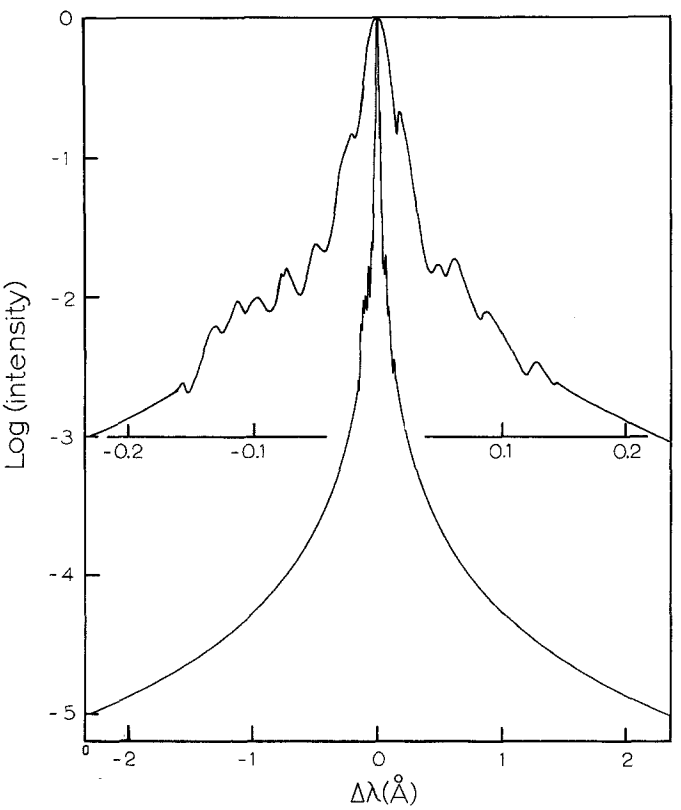

Fig. 4. The instrumental profile of the eclipse spectrograph at 4560 Å. The upper curve shows the core on an expanded wavelength scale.

transformation has advantages over previous methods (Burger and Van Cittert, 1933; Van de Hulst and Reesinck, 1947), apart from the simple machine implementation. It allows an asymmetric instrumental profile, and also the use of a close approximation to the 'optimum' noise-filter given by

$$\Phi(s) = \frac{P_S(s)}{P_S(s) + P_N(s)}, \tag{1}$$

where s is the Fourier frequency variable and P_S and P_N are the true signal and noise powers, respectively.

I refer the reader to the excellent review of Fourier restoration procedures by Brault and White (1971), and discuss only aspects in which the eclipse spectrograms differ from their examples. The correction for the instrumental profile is unusually large and the noise level also, so that instability poses a problem. In other words, the transform of the instrumental profile is not much wider than P_S and intersects the observed power spectrum close to the point where $P_S \approx P_N$ so that the division of the transforms causes noise enhancement already at low frequencies. Consequently, optimum filtering is required.

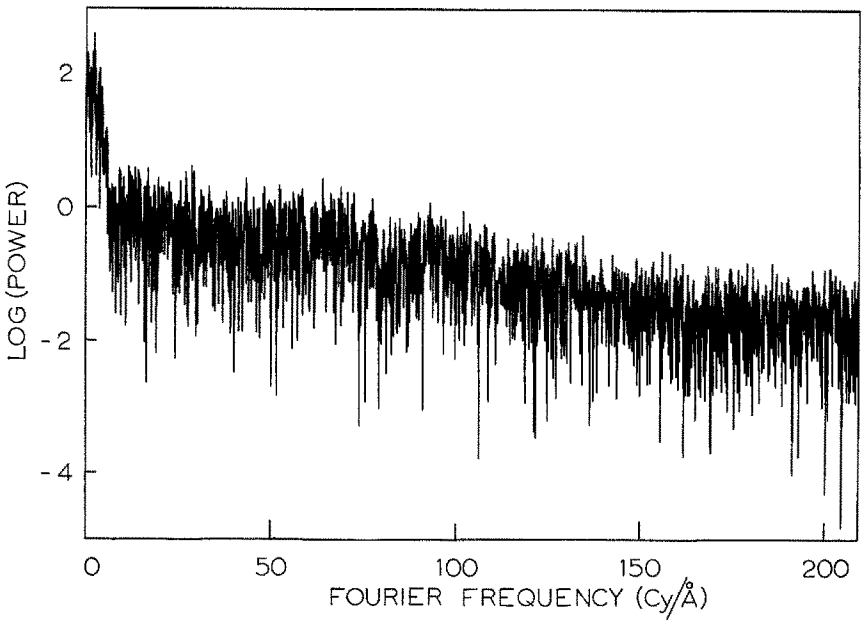

Fig. 5. Power spectrum for part of spectrogram 25.

An example of the measured power spectrum is given in Figure 5. Tapering windows were applied at the ends of the 4096-point data segments. Various noise components were identified from scans of homogeneously exposed film and scans without any film in the microphotometer. Their pattern is more clearly seen in Figure 6 which shows an average of four transforms. The steep rise at left represents the spectral lines and has the expected shape ($\sim$transform of Voigt profile: $P_S(s) \sim \exp(-as^2 - b|s|)$). The constant power above 150 cy/Å is white noise due to the microphotometry, especially to the low digitizing resolution of 8 bits only. The gradual slope in the middle is due to photographic grain. This contribution extends to high Fourier frequencies. It necessitates the small sampling interval of 4 μm (or a high Nyquist frequency above 150 cy/Å, here at 212 cy/Å), to avoid aliassing. Not only the lines but also the grains must be oversampled! The noise contribution was found to decrease below 10 cy/Å. The optimum filter was determined from averaged power spectra with a low-frequency extrapolation of the noise power based on the grain-only tracings.

The instrumental profile was normalized in the measurement domain and the Fourier shift theorem (Bracewell, 1965, p. 104) was applied to center it in the Fourier domain. The effects of the restoration are illustrated in Figure 7. The lowest trace shows the result when the inverse filter $(1-\Phi(s))$ is applied, demonstrating that no signal is lost. However, this does not imply that no noise remains. The lowest trace shows also the reduced granularity for low intensities, which in principle invalidates the optimum filter given by (1). This expression is based on the condition that signal and noise fluctuations are not correlated,

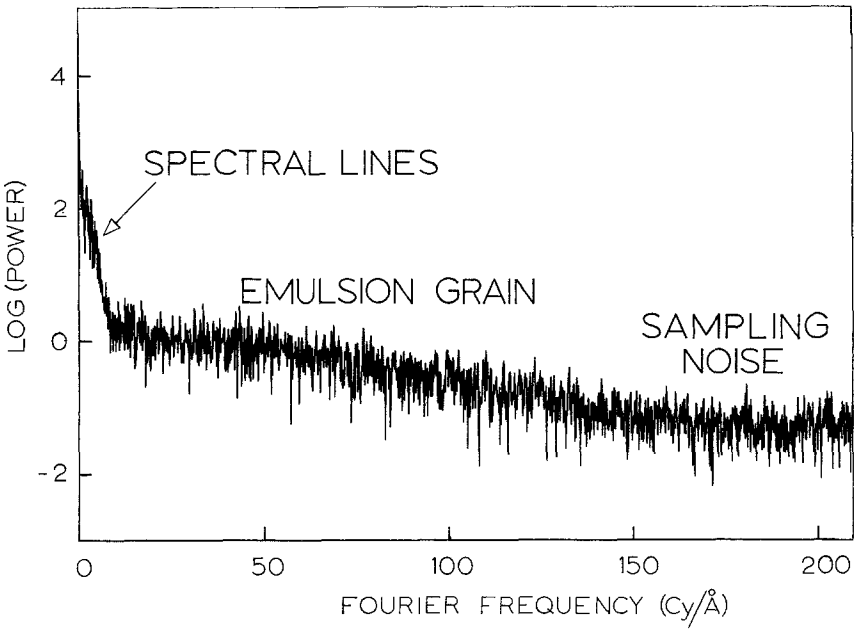

Fig. 6. Average of the power spectra of four segments of spectrogram 25. Various components are indicated.

whereas emulsion granularity depends on incident intensity. In principle it would be better to filter the line cores and the continuum separately (for instance by convolution in the measurement domain with the reverse transforms of two separately determined optimum filters). However, the quality of the present observations does not warrant such sophistication.

The whole restoration procedure was checked on calibration spectrograms taken at the center of the disk after the eclipse. Long microphotometer slits could be used to reduce the noise level. The restored scans were compared to photoelectric double-pass scans from the Jungfraujoch spectrometer, kindly provided by Dr L. Neven (Royal Observatory, Uccle-Brussels). The central depths of various lines were compared and found to agree quite well: to within 4% of the continuum intensity, while the restoration introduces corrections of up to 15%. Near the limb where the lines are weaker and wider the corrections are not so large (5–10%).

6. Tabulation of Profiles

The scatter from scan to scan is still appreciable after the noise filtering, due to low-frequency noise and to errors in the local continuum levels and in the photometric calibration. I have used the redundancy in the number of spectrograms to increase the precision of the profiles. This was possible over most of the height range where the true changes in the profiles are smaller than the observed

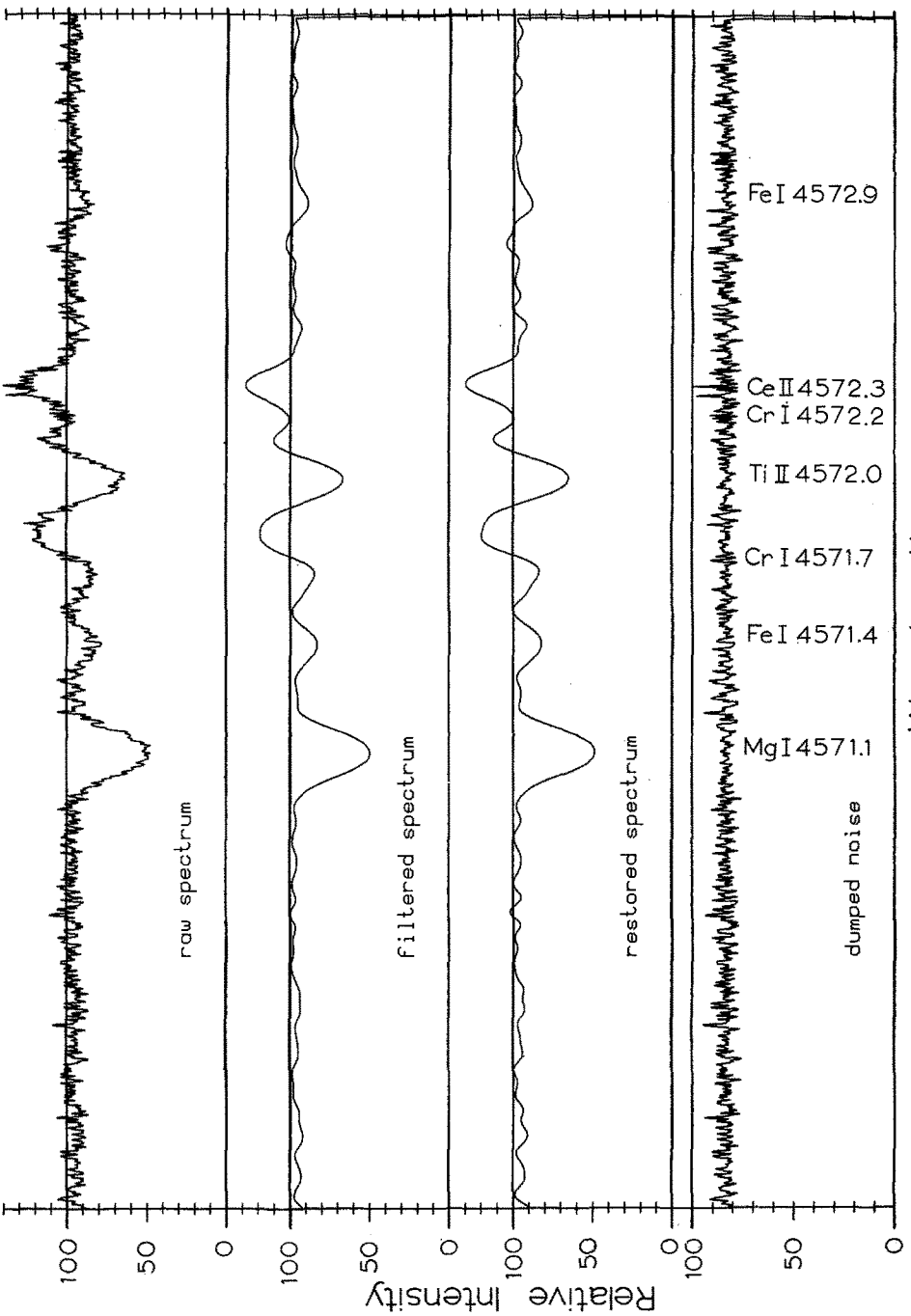

Fig. 7. Example of the Fourier restoration (part of spectrogram 25).

scatter. The positions of the centers of the λ 4554 and λ 4571 lines were determined on the restored tracings from the location of the zero of a third-order least-squares fit to the derivative of the profile, defined by $I_{k+2}-I_{k-2}$ where k counts the 4 μm samples. The profiles were subsequently sampled at multiples of 10 mÅ from line center. Tables of the variation of $I(\Delta\lambda)$ with $1/\mu$ were thus determined, where μ is the cosine of the viewing angle θ of the projected lunar limb at mid-exposure (θ is the angle between the line of sight and the local normal to the solar surface). Examples are given in Figures 8 and 9. The variable $1/\mu$ permits a better representation by low-order polynomials than the height. Second-order polynomial fits were determined by multiple regression (cf. Davies and Goldsmith, 1972, p. 276). The profiles for $1/\mu > 22$ (height > -500 km: spectra 26, 27 and 28) were not included since for these the true changes in the profiles are larger than the scatter. From the polynomial fits final profiles were obtained. They are given in Tables II and III and in Figures 10 and 11. They are spaced equidistantly in $1/\mu$ to facilitate inversion of the center-to-limb variation (cf. White *et al.*, 1972. The scaling constant A in their definition (2) is unity.).

95% confidence limits (Student's t-test) are included in the tables. They estimate the reliability of the profiles with regard to the observed scatter, but may

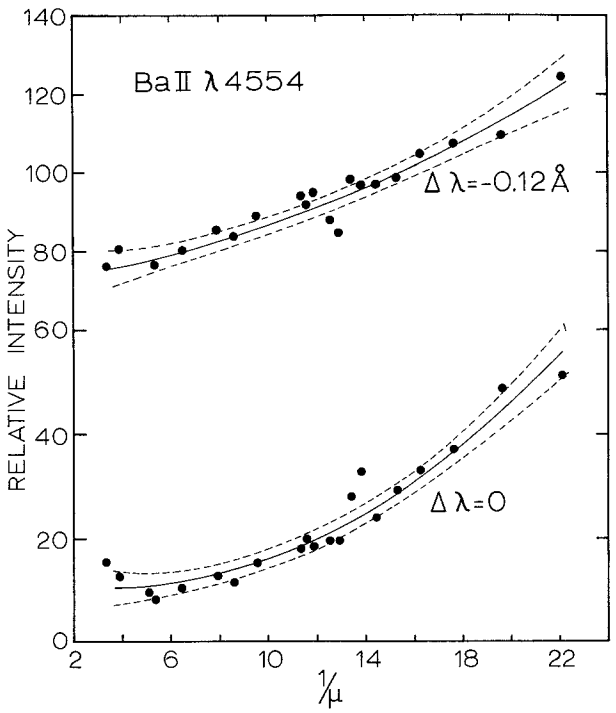

Fig. 8. Measured intensities at two wavelengths in the profile of Ba II λ 4554, relative to the local continuum (dots). The polynomial fits (full lines) and the 95% confidence levels (dashed lines) are indicated.

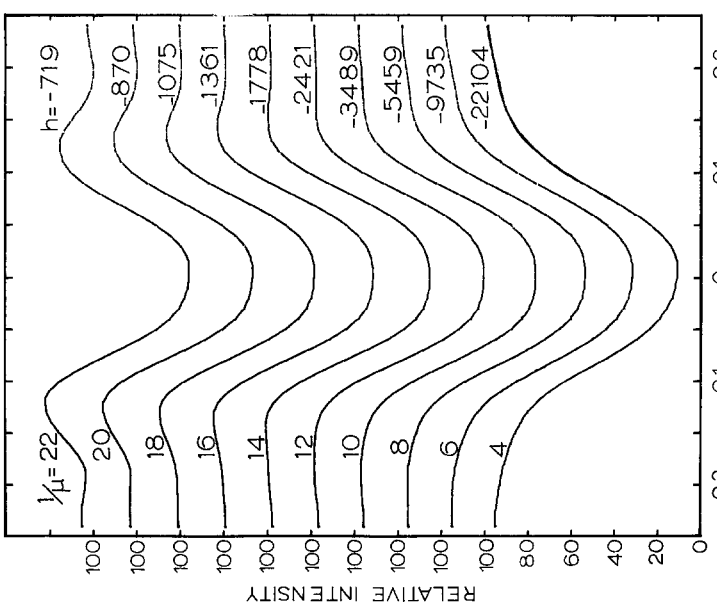

Fig. 9. Measured intensities at two wavelengths in the profile of Mg I λ 4571. Labeling as for Figure 8.

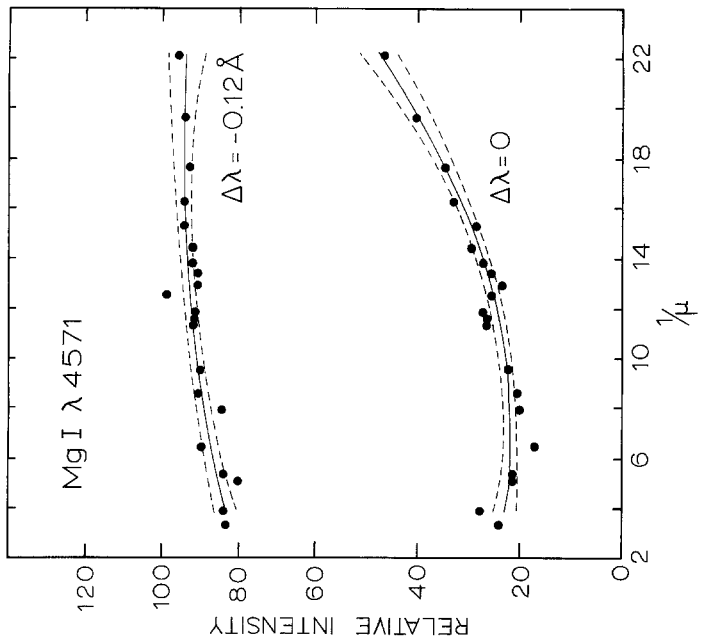

Fig. 10. Profiles of Ba II λ 4554 from the extreme limb. Ordinate: relative intensity (continuum = 100); vertical shifts of 20% per profile. Abscissa: relative wavelength.

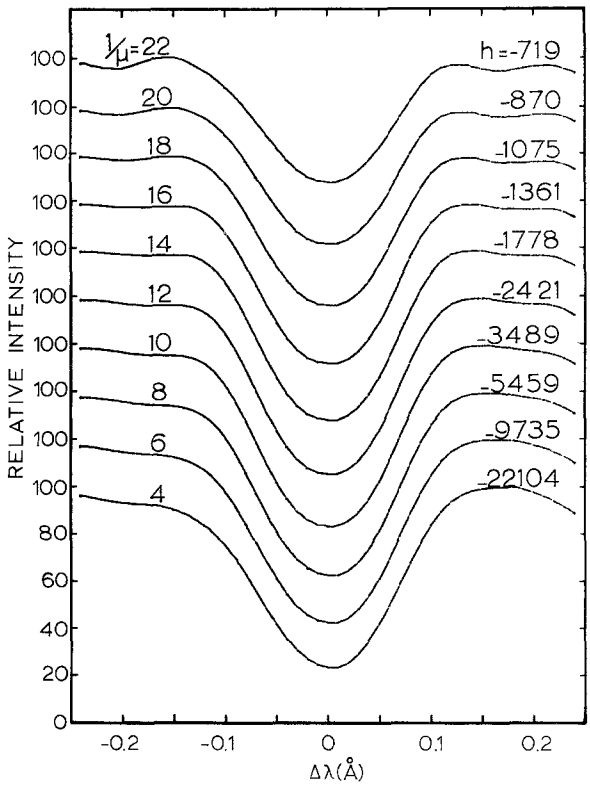

Fig. 11. Profiles of Mg I λ 4571 from the extreme limb. Labeling as for Figure 10.

underestimate the true errors since systematic errors are possibly present in the restoration and in the photometric calibration (Section 4).

An estimate of the systematic errors is obtained by comparing the eclipse profiles of the λ 4571 line to the profiles published by White *et al.* (1972) for the region of overlap. The latter are the result of time-averaged photoelectric scans made with the spectrometer at the McMath telescope and may be regarded here as ideal. Figure 12 shows the comparison. The agreement is very good. The differences exceed the 95% confidence limits appreciably only in the far wings. Systematic calibration errors due to overexposure were indeed feared for high intensities (cf. Section 4); fortunately the overexposure decreases towards the limb so that the systematic errors are not at all serious. However, they will be larger for the wings of the λ 4554 line.

Finally, Figures 13 and 14 show parts of restored scans of spectrograms 26, 27 and 28. Their reliability is lower because no least-squares fitting procedure was applied. Also, it should be noted that the uncertainty in the zero point of the height scale ($\lesssim 100$ km) is important in the interpretation of these profiles, especially for the continuum, and that the only truly chromospheric spectrogram

TABLE II

Profiles of the Ba II λ 4554.0 line at the extreme limb, including 95% confidence levels.
All values are relative to the continuum intensity (= 1000)

$1/\mu$	4	6	8	10	12	14	16	18	20	22
Height (km)	−22104	−9735	−5459	−3489	−2421	−1778	−1361	−1075	−870	−719
Δλ (mÅ)										
−250	954±29	953±20	954±16	959±16	965±17	975±17	987±18	1002±22	1019±32	1040±46
−240	951±24	950±16	952±13	957±13	964±14	975±14	989±15	1006±18	1026±26	1049±38
−230	947±22	948±15	951±12	957±12	966±13	978±13	992±14	1009±17	1028±24	1051±35
−220	941±24	946±16	952±13	961±13	970±14	982±14	995±15	1010±19	1027±26	1045±39
−210	935±27	945±18	955±14	965±14	976±15	987±15	999±16	1011±20	1023±29	1036±42
−200	928±27	942±18	956±15	969±15	981±15	992±16	1002±16	1012±20	1020±29	1028±42
−190	919±27	937±18	954±14	970±15	983±15	995±16	1006±16	1015±20	1022±29	1028±42
−180	908±26	929±18	948±14	966±14	982±15	997±15	1011±16	1023±20	1033±28	1042±41
−170	894±26	917±17	938±14	959±14	980±15	1000±15	1019±16	1037±20	1055±28	1072±41
−160	878±27	902±18	926±15	951±15	976±15	1002±16	1029±16	1055±20	1083±29	1111±42
−150	859±30	884±20	912±16	941±16	972±17	1005±17	1039±18	1075±23	1113±33	1153±47
−140	835±34	863±23	893±18	927±19	963±20	1002±20	1045±21	1090±26	1138±37	1190±54
−130	804±38	833±26	866±21	903±21	945±22	990±22	1040±23	1094±29	1152±41	1214±60
−120	760±42	790±28	825±23	865±23	910±24	961±24	1018±25	1079±32	1146±45	1219±66
−110	701±44	730±29	765±24	807±24	856±25	911±25	973±27	1014±33	1116±47	1197±69
−100	628±43	654±29	688±23	730±23	780±25	837±25	903±26	976±33	1058±47	1147±68
−90	543±41	565±27	597±22	637±22	686±23	745±24	812±25	889±31	975±44	1069±64
−80	455±38	472±25	499±20	536±21	584±22	642±22	710±23	788±29	877±41	976±60
−70	371±36	382±24	404±19	437±20	482±21	538±21	606±22	685±27	775±39	877±57
−60	297±36	302±24	320±19	349±19	391±20	445±21	511±22	590±27	680±39	783±56
−50	236±36	238±24	252±19	279±19	318±20	370±21	434±22	511±27	601±38	703±56
−40	189±35	189±23	201±19	227±19	264±20	315±20	378±21	454±26	542±38	643±55

−30	155±34	155±23	168±18	193±18	230±19	279±20	341±21	415±26	501±36	600±53
−20	129±33	132±22	147±18	173±18	210±19	260±19	321±20	393±25	478±36	574±52
−10	114±33	119±22	136±18	163±18	202±19	251±19	312±20	383±25	466±35	559±51
0	106±32	114±22	132±17	161±18	200±18	250±19	310±20	380±24	461±35	553±51
10	106±32	116±21	136±17	166±17	205±18	255±19	315±20	384±24	464±35	553±50
20	117±33	126±22	146±18	175±18	215±19	265±19	325±20	395±25	476±35	566±52
30	140±34	148±23	166±18	195±18	235±19	285±20	346±21	418±26	500±37	593±54
40	179±35	184±23	200±19	229±19	268±20	320±20	382±21	457±26	543±37	640±54
50	233±34	236±23	251±19	278±19	319±20	371±20	436±21	514±26	604±37	707±54
60	301±33	303±22	318±18	346±18	387±19	441±19	509±20	589±25	683±36	789±52
70	381±32	384±22	401±17	430±18	472±18	528±19	596±20	678±24	772±35	879±51
80	466±32	473±21	493±17	525±17	568±18	624±19	692±19	772±24	864±34	968±50
90	550±32	564±21	588±17	623±17	667±18	722±19	787±20	863±24	948±35	1044±50
100	629±32	650±21	679±17	716±17	761±18	813±19	874±20	942±24	1018±35	1102±50
110	699±31	726±21	759±17	797±17	841±18	890±18	944±19	1003±24	1068±34	1138±50
120	759±30	790±20	824±16	862±16	902±17	946±17	993±18	1043±23	1096±32	1152±47
130	808±27	840±18	873±15	907±15	943±16	981±16	1020±17	1061±21	1103±29	1147±43
140	848±25	877±16	906±13	936±13	966±14	996±14	1028±15	1059±19	1092±27	1124±39
150	879±24	903±16	927±13	951±13	975±14	998±14	1022±15	1045±18	1069±26	1092±38
160	901±27	921±18	940±14	958±15	976±15	993±16	1010±16	1026±20	1041±29	1056±42
170	916±30	932±20	947±16	961±16	974±17	986±17	997±18	1007±22	1016±32	1024±46
180	927±30	940±20	952±16	963±16	973±17	981±17	988±18	994±23	999±32	1002±47
190	938±28	949±19	958±15	967±15	974±16	980±16	985±17	989±21	992±30	994±44
200	951±26	958±17	965±14	971±14	977±15	982±15	987±16	991±20	994±28	997±41
210	965±26	969±17	973±14	977±14	981±15	986±15	991±16	996±20	1001±28	1007±41
220	978±27	978±18	979±15	981±15	984±15	989±16	994±16	1001±20	1009±29	1018±43
230	987±28	984±18	983±15	983±15	986±16	990±16	997±17	1004±21	1014±30	1026±43
240	986±29	983±19	982±15	983±16	986±16	990±17	997±18	1006±22	1016±31	1028±45

TABLE III

Profiles of the Mg I λ 4571.1 line at the extreme limb, including 95% confidence levels.
All values are relative to the continuum intensity (= 1000)

$1/\mu$	4	6	8	10	12	14	16	18	20	22
Height (km)	−22104	−9735	−5459	−3489	−2421	−1778	−1361	−1075	−870	−719
Δλ (mÅ)										
−250	972±28	975±19	979±15	981±15	983±16	985±16	986±17	986±21	986±30	986±44
−240	961±31	968±21	973±17	978±17	981±18	983±18	983±19	982±23	981±33	977±48
−230	950±32	960±21	968±17	974±17	978±18	979±18	979±19	976±24	972±34	965±50
−220	941±30	953±20	963±16	970±16	974±17	975±18	974±18	971±23	964±33	955±48
−210	934±26	947±18	957±14	964±14	969±15	971±15	970±16	967±20	961±28	952±41
−200	929±21	941±14	951±11	959±11	964±12	967±12	968±13	967±16	964±23	958±33
−190	925±19	936±13	945±10	953±10	960±11	965±11	968±12	971±14	971±20	970±30
−180	922±21	932±14	941±11	949±11	956±12	963±12	970±13	976±16	981±23	985±33
−170	919±25	928±16	937±13	946±13	955±14	963±14	972±15	980±19	988±27	997±39
−160	912±26	923±18	934±14	944±14	955±15	964±15	974±16	983±20	993±28	1001±41
−150	901±26	917±18	931±14	944±14	955±15	966±15	975±16	983±20	990±28	996±41
−140	885±26	906±18	925±14	940±14	954±15	964±15	973±16	978±20	982±28	982±41
−130	864±27	890±18	912±15	930±15	945±16	956±16	963±17	966±21	966±30	962±43
−120	836±30	865±20	889±16	909±16	925±17	936±17	943±18	946±22	944±32	937±47
−110	799±32	828±22	853±17	874±18	890±18	902±19	910±20	914±24	913±35	909±51
−100	752±34	778±23	801±18	821±18	838±19	851±20	862±21	869±26	873±37	874±53
−90	696±34	716±23	735±18	752±18	769±19	784±20	798±21	811±26	823±37	834±53
−80	629±31	642±21	656±17	671±17	687±18	704±18	723±19	743±24	763±34	785±49
−70	557±27	562±18	571±15	583±15	599±15	618±16	641±16	667±20	697±29	730±42
−60	484±23	482±15	486±12	496±13	511±13	532±13	559±14	591±17	629±25	673±36
−50	414±21	407±14	407±12	415±12	430±12	453±12	483±13	520±16	565±23	617±34

−40	352±22	342±15	340±12	347±12	363±12	386±13	419±13	459±17	509±24	566±34
−30	302±22	290±15	288±12	295±12	311±13	335±13	369±14	412±17	464±24	525±35
−20	264±22	253±15	251±12	258±12	275±13	300±13	335±14	379±17	432±24	495±35
−10	240±22	230±15	229±12	237±12	254±13	281±13	316±14	360±17	414±24	477±35
0	229±22	220±15	220±12	229±12	147±13	274±13	310±14	355±17	409±24	471±35
10	233±22	225±15	225±12	235±12	253±13	280±13	316±14	362±17	416±24	479±35
20	254±22	245±15	245±12	254±12	272±12	299±13	335±13	380±16	433±23	496±34
30	293±21	283±14	282±11	290±11	307±12	333±12	368±13	412±16	465±23	526±33
40	348±22	338±14	337±12	345±12	361±12	385±13	418±13	459±16	509±23	567±34
50	417±24	410±16	410±13	418±13	433±14	456±14	486±15	523±18	567±26	619±37
60	498±28	495±19	499±15	507±15	522±16	542±16	568±17	600±21	638±30	681±44
70	586±32	589±22	595±18	606±18	620±19	639±19	661±20	687±25	717±35	751±51
80	675±36	683±24	693±19	705±19	719±20	735±21	753±22	773±27	795±39	820±56
90	759±36	770±24	782±20	794±20	807±21	821±21	835±22	849±27	864±39	880±57
100	833±33	845±22	857±18	868±18	879±19	889±19	899±20	909±25	918±36	927±52
110	893±28	904±19	914±15	923±15	931±16	938±16	944±17	949±21	953±31	956±44
120	937±24	946±16	953±13	960±13	965±14	968±14	970±15	971±18	970±26	968±38
130	966±22	972±15	977±12	980±12	982±13	982±13	981±13	978±17	973±24	967±35
140	984±22	987±15	989±12	990±12	988±13	985±13	981±14	975±17	969±24	957±35
150	993±23	993±15	992±12	990±13	986±13	981±13	974±14	966±17	957±25	946±36
160	998±23	984±15	990±12	985±12	979±13	972±13	965±14	957±17	949±25	939±36
170	998±22	991±15	985±12	978±12	971±12	965±13	958±13	952±17	946±24	940±34
180	994±21	986±14	978±11	971±11	965±12	960±12	956±13	952±16	950±23	948±33
190	985±21	978±14	971±11	966±11	962±12	959±12	957±13	956±16	957±23	958±33
200	971±23	967±15	964±12	962±12	960±13	960±13	960±14	961±17	963±24	965±35
210	954±24	955±16	956±13	957±13	958±14	959±14	961±15	963±18	965±26	967±38
220	934±25	939±17	944±14	947±14	951±14	954±15	956±15	958±19	959±27	960±40
230	912±25	919±17	926±14	932±14	937±14	941±15	944±15	946±19	947±27	947±40
240	887±24	895±16	902±13	909±13	914±14	919±14	923±15	927±18	929±26	931±38

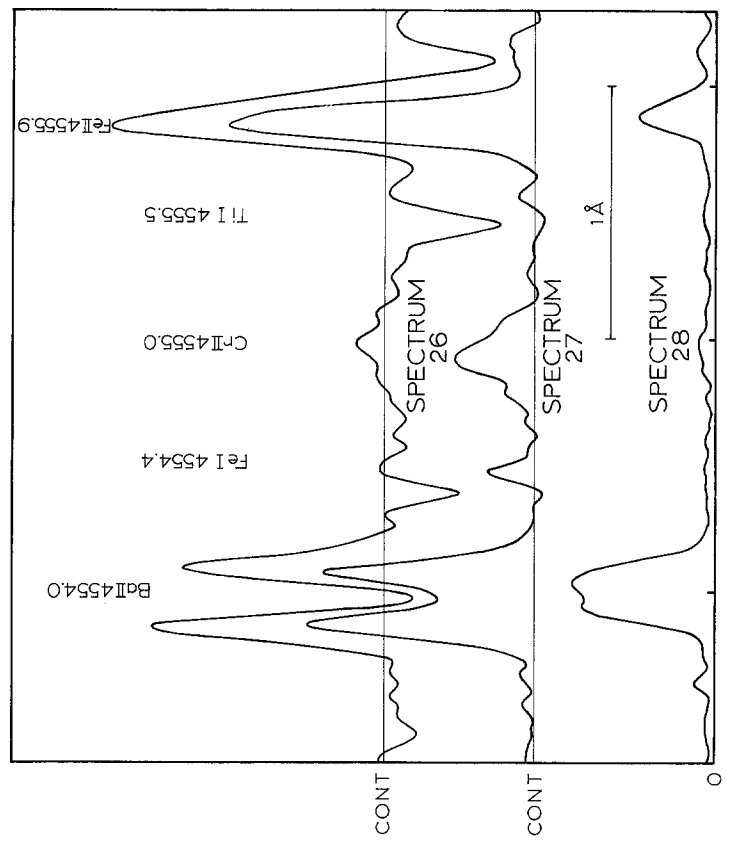

Fig. 13. Parts of the restored scans of spectrograms 26, 27 and 28 around Ba II λ 4554. The relative intensity scale differs per tracing (zero intensity common to all tracings). The wavelength scale is relative for each tracing.

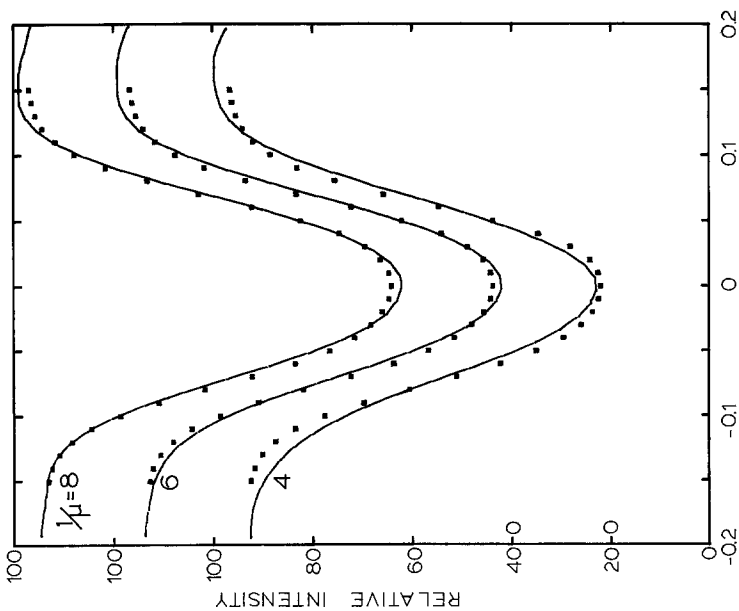

Fig. 12. Comparison of eclipse profiles with Kitt Peak observations (squares) for Mg I λ 4571.

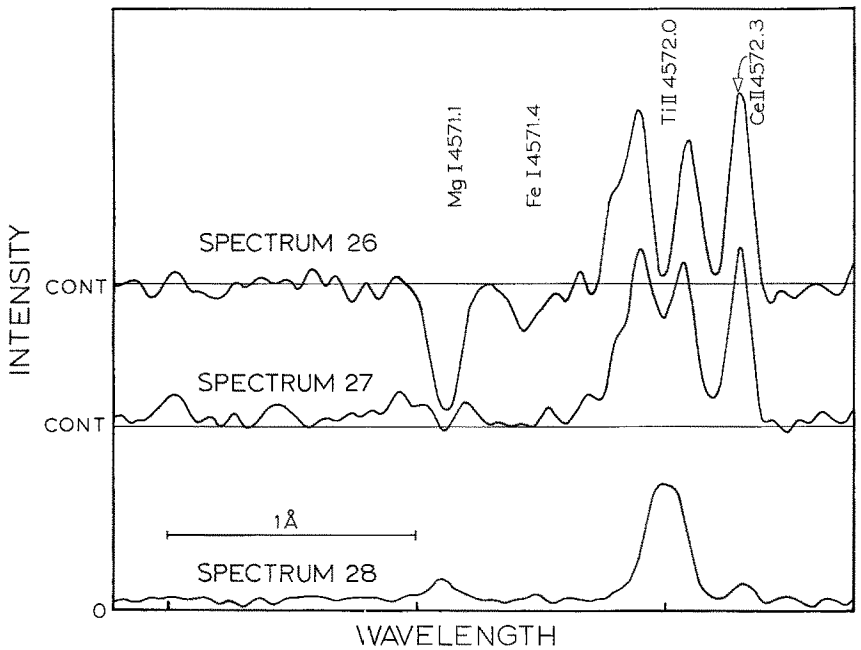

Fig. 14. Parts of the restored scans of spectrograms 26, 27 and 28 around Mg I λ 4571. Labeling as for Figure 13.

(No. 28) was an 8.7 s exposure. During this time the Moon covered 2400 km, more than the full emission height of the two lines.

7. Discussion

The observations given here represent the first spectral line data from the extreme limb in the form of detailed profiles. Their precision is sufficient for detailed analysis.

The contrast in behaviour of the two lines is remarkable. The Mg I λ 4571 'LTE' line stays in absorption throughout the outer limb (Figure 11). The minute emission wings shown at $1/\mu \approx 20$ are not significant. The line turns abruptly into emission at the limb (Figure 14). The slight self-absorption shown in its core on spectrogram 27 is barely significant.

The Ba II λ 4554 K-like resonance line exhibits line wings in emission above the local continuum already at $1/\mu = 16$, or 1400 km within the limb (Figure 10). These emission wings are definitely significant, and will be analysed in a subsequent paper.

At the limb the line becomes a strong self-absorbed emission line, and shows asymmetry in its two emission peaks (Figure 13).

Acknowledgements

I am indebted to H. J. van Amerongen and H. Jansen for help with the modernization of the 'old' microphotometer, to G. W. Geijtenbeek and E. B. J. van der Zalm for help with the computations, to Edith Müller, O. Namba, J. W. Wijbenga and especially C. Zwaan for discussions, and to R. J. Bessey, O. Namba and C. Zwaan for comments on the paper.

The eclipse expedition to the March 7, 1970 eclipse was supported by the Netherlands Organization for the Advancement of Pure Research (Z.W.O.)

References

Altrock, R. C. and Canfield, R. C.: 1974, *Astrophys. J.* **194,** 733.
Altrock, R. C. and Cannon, C. J.: 1972, *Solar Phys.* **26,** 21.
Altrock, R. C. and Cannon, C. J.: 1973a, *Solar Phys.* **29,** 275.
Altrock, R. C. and Cannon, C. J.: 1973b, *Solar Phys.* **30,** 31.
Altrock, R. C. and Cannon, C. J.: 1975, *Solar Phys.* **42,** 289.
Athay, R. G. and Canfield, R. C.: 1969, *Astrophys. J.* **156,** 695.
Bracewell, R.:1965, *The Fourier Transform and its Applications*, McGraw-Hill, New York.
Brault, J. W. and White, O. R.: 1971, *Astron. Astrophys.* **13,** 169.
Breckinridge, J. B.: 1971, *Appl. Opt.* **10,** 286.
Burger, H. C. and Van Cittert, P. H.: 1933, *Z. f. Phys.* **81,** 428.
Davies, O. L. and Goldsmith, P. L.: 1972, *Statistical Methods in Research and Production*, Oliver and Boyd, Edinburgh.
Dunn, R. B., Evans, J. W., Jefferies, J. T., Orrall, F. Q., White, O. R., and Zirker, J. B.: 1968, *Astrophys. J. Suppl.* **15,** no. 139, 275.
Griffin, R. F.: 1969, *Monthly Notices Roy. Astron. Soc.* **143,** 319.
Hansen, R. T., Hansen, S. F., and Garcia, Ch. J.: 1970, *Solar Phys.* **15,** 387.
Houtgast, J.: 1948, *Bull. Astron. Inst. Neth.* **10,** 417.
Houtgast, J. and Namba, O.: 1975, *Proc. First European Solar Meeting. Osserv. Mem. Osserv. Astrof. Arcetri* **105,** 115.
Houtgast, J., Namba, O., and Rutten, R. J.: 1976, *Proc. Kon. Ned. Akad. Wetensch., Amsterdam, B* **79,** 221 (Paper I).
Houtgast, J., Namba, O., Rutten, R. J., and Wijbenga, J. W.: 1971, *Solar Phys.* **21,** 281.
Livingston, W. C. and White, O. R.: 1974, *Solar Phys.* **39,** 289.
Redman, R. O.: 1943, *Monthly Notices Roy. Astron. Soc.* **103,** 173.
Redman, R. O.: 1955, *Vistas in Astronomy* **1,** 713.
Rutten, R. J.: 1973, *Solar Phys.* **28,** 347.
Rutten, R. J. and Van Amerongen, H. J.: 1975, in C. de Jager and H. Nieuwenhuijzen (eds.), *Image Processing Techniques in Astronomy*, D. Reidel, Dordrecht, Holland, p. 261.
Singleton, R. C.: 1968, *Comm. ACM*, **11,** 773.
Van de Hulst, H. C. and Reesinck, J. J. M.: 1947, *Astrophys. J.* **106,** 121.
White, O. R., Altrock, R. C., Brault, J. W. and Slaughter, C. D.: 1972, *Solar Phys.* **23,** 18.
Wijbenga, J. W. and Zwaan, C.: 1972, *Solar Phys.* **23,** 265.